https://doi.org/10.5194/hess-2020-291
Preprint. Discussion started: 10 July 2020

Hydrology and Earth System Sciences
Discussions

Soil dielectric characterization at L-band microwave frequencies during freeze-thaw transitions

Alex Mavrovic[1-2], Renato Pardo Lara[3], Aaron Berg[3], François Demontoux[4], Alain Royer[5-2], Alexandre Roy[1-2]

[1] Université du Québec à Trois-Rivières, Trois-Rivières, Québec, G9A 5H7, Canada
[2] Centre d'Études Nordiques, Université Laval, Québec, Québec, G1V 0A6, Canada
[3] University of Guelph, Guelph, Ontario, N1G 2W1, Canada
[4] Laboratoire de l'Intégration du Matériau au Système, Bordeaux, 33400 Talence, France
[5] Centre d'Applications et de Recherches en Télédétection, Université de Sherbrooke, Sherbrooke, Québec, J1K 2R1, Canada

Correspondence to: Alex Mavrovic (Alex.Mavrovic@uqtr.ca)

Abstract. Soil microwave permittivity is a crucial parameter in passive microwave retrieval algorithms but remains a challenging variable to measure. To validate and improve satellite microwave data products, precise and reliable estimations of the relative permittivity ($\varepsilon_r = \varepsilon/\varepsilon_0 = \varepsilon' - j\varepsilon''$; unitless) of soils are required, particularly for frozen soils. In this study, permittivity measurements were acquired using two different instruments: the newly designed open-ended coaxial probe (OECP) and the conventional Stevens HydraProbe. Both instruments were used to characterize the permittivity of soil samples undergoing several freeze/thaw cycles in a laboratory environment. The measurements were compared to soil permittivity models. We show that the OECP is a suitable device for measuring frozen (ε'_{frozen} = [3.5;6.0], ε''_{frozen} = [0.4;1.2]) and thawed (ε'_{thawed} = [6.5;22.8], ε''_{thawed} = [1.4;5.7]) soil microwave permittivity. We also demonstrate that cheaper and widespread soil permittivity probes operating at lower frequencies (i.e. Stevens HydraProbe) can be used to estimate microwave permittivity given proper calibration relative to an L-band (1–2 GHz) probe. This study also highlighted the need to improve dielectric soil models, particularly during freeze/thaw transitions. There are still important discrepancies between *in situ* and modelled estimates and no current model accounts for the hysteresis effect shown between freezing and thawing processes which could have a significant impact on freeze/thaw detection from satellites.

Keywords: Open-ended coaxial probe, Freeze-thaw cycles, Soil permittivity, Microwave radiometry, Soil emission modelling

1 Introduction

The current generation of L-band (1–2 GHz) satellite-based radiometers offers a unique opportunity to monitor soil moisture and freeze/thaw cycles due to its global coverage and revisit time of only a few days (Kerr et al., 2012; Roy et al., 2015; Rautiainen et al., 2016; Colliander et al. 2017; Derksen et al., 2017; Wigneron et al., 2017). These satellites include the European Space Agency Soil Moisture Ocean Salinity mission (SMOS; Kerr et al., 2010), the National Aeronautics and Space Administration (NASA) Soil

https://doi.org/10.5194/hess-2020-291
Preprint. Discussion started: 10 July 2020

Moisture Active Passive mission (SMAP; Entekhabi et al., 2010) and the NASA/CONAE (Comisión Nacional de Actividades Espaciales) joint Aquarius mission (Le Vine et al., 2010). Information about the physical state of the soil is retrieved from microwave observations by using radiative transfer models to simulate the interaction between electromagnetic waves and the surface. Such models have already been applied to obtain information on the characteristics of snow cover (Lemmetinen et al., 2016), the state of vegetation (Mo et al., 1982; Rodríguez-Fernández et al., 2018, Fan et al., 2018), soil moisture (Kerr et al., 2012; Mialon et al., 2015; Colliander et al. 2017) and soil freeze/thaw state (Kim et al., 2012; Rautiainen et al., 2016; Derksen et al., 2017; Roy et al., 2017a, 2018 and 2020; Prince et al., 2019).

Permittivities of the landscape constituents are crucial components of the dielectric models used to solve the electromagnetic equations governing the interaction between microwave and surface. The permittivity of a medium (ε, in F/m) determines its behavior when exposed to an electric field. The relative permittivity is the ratio between a medium's permittivity and that of a vacuum ($\varepsilon_r = \varepsilon/\varepsilon_0 = \varepsilon' - i\,\varepsilon''$; unitless; hereafter relative permittivity will stand for permittivity). Permittivity is characterized by a complex number, where the real part (ε') describes the reorientation of molecular dipoles, which drives wave propagation, and the imaginary part (ε'') describes the absorption (or loss) of energy. The real and imaginary parts are linked through the Kramers–Kronig relations (Klingshirn, 2012), therefore they are not fully independent. A medium that strongly opposes the application of an external electric field displays a high permittivity (e.g. $\varepsilon'_{water} \approx 78–79$ in the 1–2 GHz frequency range; Pavlov and Baloshin, 2015) and a medium that does not strongly oppose an external electric field displays a low permittivity (e.g. $\varepsilon'_{air} \approx 1$).

Because of water's high permittivity, it dominates the microwave signal observed by satellite-based radiometers. Similarly, soil moisture retrieval algorithms exploit the high contrast in water-soil-air permittivity differences. However, the water phase also plays an important role in soil permittivity. When water freezes, the molecules become bound in a crystal lattice and the permittivity drops drastically compared to liquid water (i.e. $\varepsilon'_{ice} \approx 3$). The permittivity drop observable within freezing soils translates into a higher passive microwave emission from the ground. This allows for the retrieval of the ground state (freeze/thaw) from passive microwave observations (Rautiainen et al. 2012; Roy et al., 2015; Derksen et al, 2017). Soil permittivity is especially important in radiative transfer models since it acts as a boundary condition in the models. As microwave permittivity is challenging to measure in field settings, it is typically derived from empirical relationships and physical properties. Nonetheless, many uncertainties remain in the relationship between soil permittivity and soil physical parameters (Montpetit et al., 2018; Moradizadeh and Saradjian, 2016). This is especially evident during the winter when, in many cases, fixed values are introduced in data analysis algorithms due to a lack of better estimates or, in other cases, data are simply not available during winter. The high uncertainties in soil permittivity models result from the difficulty in gathering *in situ* permittivity data at microwave frequencies to parameterize and validate these models. This is further complicated by the frequency dependence of permittivity.

https://doi.org/10.5194/hess-2020-291
Preprint. Discussion started: 10 July 2020

Therefore, there is a need to collect permittivity estimates for the validation of passive microwave instruments. However, the majority of instruments deployed to validate microwave permittivity models, such as soil moisture sensors, use measurement frequencies (50–70 MHz) well outside the range of the concerned satellite observations (1400–1427 MHz). Until now, in the absence of a better alternative, the assumption that MHz and L-Band microwave soil permittivity are equivalent has been widely used to validate SMAP and SMOS algorithms (Roy et al., 2017a; Lemmetyinen et al., 2016), although this assumption was never rigorously tested. Furthermore, very few instruments used in field conditions continuously measure microwave permittivity in the frequency range of satellite sensors (Demontoux et al., 2019 and accepted). In addition, only a few laboratory studies have used L-Band permittivity measurements, and most of the available studies have focused on thawed soil samples (Bircher et a., 2016a and 2016b; Demontoux et al., 2017).

The goal of this laboratory-based study is to assess L-band permittivity measurements in frozen soils and the implications of substituting them with permittivity estimates taken at lower frequency by: 1) evaluating the L-band permittivity of different types of soil in frozen and unfrozen conditions using an open-ended coaxial probe (OECP); 2) comparing the OECP measurements with those from a commercially available soil moisture probe operating at a lower frequency (i.e. the Stevens HydraProbe) to evaluate the potential of these lower cost probes to estimate L-Band permittivity, and; 3) comparing the soil permittivity measurements captured with both devices against that predicted from soil permittivity models currently used in L-band passive microwave retrieval algorithms. This paper is structured as follows: Section 2.1 describes permittivity instruments used in this study; Section 2.2 gives an overview of soil permittivity models used for satellite retrieval; Section 3 provides information on the study sites, data collection and laboratory setup. Lastly, in Sections 4 and 5, we compare and contrast the OECP measurements, commercial probe measurements and model simulations.

2 Theoretical background

2.1 Soil permittivity instruments

This study compares the permittivity estimates from two devices, an OECP and the Stevens HydraProbe, the following sections briefly describe these instruments.

2.2.1 Open-Ended Coaxial Probe (OECP)

An OECP was developed by the Université de Sherbrooke (UdeS) and Université du Québec à Trois-Rivières (UQTR) to monitor the permittivity at L-band frequencies of tree trunks (Mavrovic et al., 2018) and snow (Mavrovic et al., 2020) (Fig. 1a). The OECP acts as a coaxial waveguide, and the reflection coefficient at the interface of its open edge and the probed medium is measured by a reflectometer connected to the OECP.

https://doi.org/10.5194/hess-2020-291
Preprint. Discussion started: 10 July 2020

This reflectometer acts as both a generator providing electric field propagation to the probe and a reflection coefficient measuring instrument. The reflection coefficient (i.e. magnitude of the reflected and incident electric field ratio) depends on the permittivity of the probed medium. The permittivity is retrieved from the reflection coefficient using a specific calibration based on open (air), short (copper plate) and standard samples (saline solutions of known permittivity) (Filali et al., 2006 and 2008). The permittivity of a wide range of materials can be measured by the OECP as long as it is possible to ensure the probe's open edge makes contact with a flat and smooth surface. This probe has already been described in detail and calibrated on known permittivity surfaces (Mavrovic et al., 2018 and 2020). The penetration depth of the OECP can be defined as the maximal depth at which a medium is exposed to a large enough electric field to be efficiently measured. The magnitude of this effective electric field in the medium is proportional to the medium's permittivity and depends on the electric field magnitude generated by the reflectometer, which is constant (10 dBm) (Fig. 1b). The OECP typical penetration depth approaches 1 cm under dry soil conditions and the cylindrical probed volume is about 3.5 cm wide in diameter (Figure 2). Under wet soil conditions, the penetration depth shrinks down to 0.4 cm. The probe system is operational in remote environments since it is easily transportable, sensibly sized (low weight and small dimensions), energy efficient, weatherproof, and operates at low temperatures. The OECP integrates a permittivity measurement in less than a second and does not require destructive sampling, although the user must be careful to avoid air gaps between the probe and the soil. While tested on reference solids, the OECP display uncertainties under 3.3% for real permittivity and under 2.5% or 0.04 (whichever is greater) for imaginary permittivity (Mavrovic et al., 2018).

2.2.1 HydraProbe

The HydraProbe (HP) is a commercial soil moisture probe, from *Stevens Water Monitoring Systems, Inc.,* that uses coaxial impedance dielectric reflectometry to measure soil permittivity (HydraProbes Soil Sensor User Manual, 2018). The probe consists of a cylindrical casing which houses the electronics as well as four stainless steel tines (0.3 cm in diameter, 5.7 cm long) that protrude from a metal base plate (4.2 cm diameter). Three tines are arranged in a circle 3.0 cm in diameter around a central tine. The HP operates at 50 MHz and probes a larger volume than the OECP, ranging between approximately 40 and 350 cm^3. Like the OECP, it uses the ratio of the incident and reflected waves to numerically solve Maxwell's equations, yielding the impedance and complex permittivity. Thus, the HP measures real and imaginary soil permittivities (± 0.2 or ± 1%, whichever is greater) as well as temperature (± 0.3°C). From these two variables, soil moisture is estimated using an empirical relationship calibrated for the given soil type (between ± 0.01 and 0.03 volumetric water content depending on soil type), with individual calibrations resulting in slightly lower uncertainties (Seyfried et al., 2005; Burns et al., 2014; Rowlandson et al., 2013). This probe is widely used to measure soil moisture for meteorological and agricultural applications. It is deployed along several meteorological station networks (e.g Tetlock et al. 2019). Figure 2 illustrates typical probed volumes for the OECP (dry ~10 cm^3, wet ~5 cm^3) and HP (dry ~40 cm^3, wet ~350 cm^3) under dry and wet soil conditions.

https://doi.org/10.5194/hess-2020-291
Preprint. Discussion started: 10 July 2020


Hydrology and Earth System Sciences
Discussions

2.2 Soil permittivity models

Two models commonly used in the remote sensing community for the retrieval of the soil freeze-thaw state were selected.

2.2.1 Temperature Dependable Generalized Refractive Mixing Dielectric Model (TD GRMDM)

The TD GRMDM is a semi-empirical model that estimates the microwave permittivity of a soil from its physical properties (Mironov et al., 2010). The model accounts for the effect of soil granulometry, temperature and water liquid content through empirical relationships. This model allows for the distinction of bound and free water, giving each of these components a distinct dielectric spectrum. The input parameters required in TD GRMDM are frequency (set at 1.4 GHz for this study), soil moisture, temperature, dry bulk density and clay fraction. Soil moisture is the main parameter driving soil permittivity. This model was built and validated on a soil database comprising the full range of textures covered by the SMOS mission (Mialon et al., 2015; Mironov et al., 2009 and 2010). However, with respect to the soil water freeze/thaw state, TD GRMDM is a binary model. All water in the soil is either thawed or frozen, therefore the freeze/thaw transition appears as a discontinuity. The model, however, allows for offsetting the freeze/thaw transition temperature to account for freezing point depression. TD GRMDM uses fixed values for frozen soils with no dependency on temperature, ice fraction or soil composition.

2.2.2 Zhang's Model

The model from Zhang et al. (2010) (henceforth Zhang's model) is a semi-empirical soil model for estimating microwave soil permittivity from soil physical characteristics. It is an extension of the semi-empirical mixing dielectric model (SMDM) adapted to frozen soils from Dobson et al. (1985). Zhang's model evaluates the ice fraction (f_i) in soil near the freezing point in order to obtain a smooth transition between the solid and liquid phases of water. An empirical exponential decay function ($f_i = A \cdot |T_{soil}|^{-B}$) is used to estimate the liquid water vs. ice fractions in the freezing soils. The parameters A and B of the previous function were empirically estimated based on soil type. From this ice fraction estimate, the approach uses semi-empirical dielectric mixing equations for soil water/ice mixture to estimate soil permittivity at microwave frequencies. The input parameters required by Zhang's model include frequency (set at 1.4 GHz for this study), soil moisture (main driver for soil permittivity), temperature, dry bulk density and composition (clay, silt and sand fractions) (Zhang et al., 2003 and 2010; Mironov, 2017).

3 Data and methods

3.1 Methods

Two experiments were performed in this study, the first under fast freeze/thaw transition conditions (one-time air temperature adjustment), and the second under slow transition conditions with small progressive increases in air temperature.

https://doi.org/10.5194/hess-2020-291
Preprint. Discussion started: 10 July 2020

3.1.1 Fast freeze/thaw transition

Continuous permittivity measurements were conducted on mineral and organic soil samples going through several consecutive freeze/thaw cycles in a NorLake2 mini-room walk-in controlled temperature chamber (5.55 to 19.11 m^3 volume) equipped with a CP7L control panel at the School of Environmental Science of the University of Guelph (UofG). The soil samples were collected in PVC or plastic containers. The containers were placed in an insulated cardboard box (28x38x33 cm for a volume of $3.5x10^4$ cm^3) filled with sand to surround the soil samples (Fig. 3). This setup was intended to simulate the hot/cold front coming from the surface by isolating the sides and bottom of the soil samples. The OECP and HP were fully buried and centered at a depth of 2.5 cm below the soil surface (Fig. 3). For the organic soil samples, into which multiple probes were inserted, sufficient spacing (~ 7.5 cm with the OECP and > 1 cm between the HP) between probes was ensured to avoid probe interaction.

HP output signals were logged with a CR800 datalogger and HPP output signals were logged with a CR1000 datalogger (both from Campbell Scientific, Inc.). Unlike the HP, the OECP does not record temperature. Therefore, a Campbell Scientific 107 temperature probe was placed next to the OECP to measure soil temperature. The air temperature of the cold chamber was set at +10°C for thawing cycles (initial air temperature of -10°C) and -10°C for freezing cycles (initial air temperature of +10°C). These experimental conditions allowed for a complete freeze/thaw cycle in approximately 24 hours and were chosen for practical considerations. However, it should be acknowledged that these conditions represent a relatively rapid transition. Permittivity and temperature measurements were set at one-minute intervals for all instruments.

3.1.2 Slow freeze/thaw transition

To investigate the effect of slower transitions, another experimental setup was created in a Climats EXCAL 1411-HE cold chamber (0.138 m^3 volume) at the Laboratoire de l'Intégration du Matériau au Système (Bordeaux, France). Since the soil sample and the Polytetrafluoroethylene (i.e. PTFE or TEFLON) container had smaller volumes, the OECP probe was installed on top of the soil sample with its open end in contact with the soil (Fig. 4). Only OECP permittivity measurements were taken in this experiment since an HP sensor was not available. The objective of this experimental setup was to force a slow freeze/thaw transition. Permittivity measurements were taken only when the soil temperature equilibrated with the cold chamber air temperature (± 0.1°C). This method was significantly more time-consuming than the fast transition setup, as a full cycle took several days and required heavy user surveillance.

3.2 Studied soil types

The studied soil samples were collected from four different sites and consisted of a single homogenous soil layer (Table 1). Care was taken during transportation to the cold chamber to preserve their original state and leave their structure and moisture content as undisturbed as possible.

https://doi.org/10.5194/hess-2020-291
Preprint. Discussion started: 10 July 2020

The first site was located in the boreal forest at the Old Black Spruce Research Station (OBS). This research facility is in northern Saskatchewan near Canada's boreal forest southern limit and is part of the Boreal Ecosystem Research and Monitoring Sites (BERMS). Its soil is rich in organic matter, displays high soil moisture levels for most of the thawed season (Gower et al., 1997), and is further described in Roy et al. (2020). The samples were collected in January 2018.

The remaining sites were all in agricultural fields with mineral soils in southern Ontario, Canada. Soil samples were collected at the University of Guelph's Elora Research Station (sandy loam; collected late fall 2017) as well as on private farms in Cambridge (loamy sand; collected late fall 2017) and Dunnville (clay loam; collected mid-winter 2018). The soils were selected to be representative of a range of soil textures and complement existing research at the three locations. These samples and their collection process are further described in Pardo Lara et al. (2020) and the data are available at the Federated Research Data Repository through the Polar Data Catalog of metadata (PDC; https://dx.doi.org/10.20383/101.0200).

The soil composition and liquid water content of each sample were analyzed (Table 1). A particle size analysis of the OBS sample was completed at the UdeS using a soil sifting approach to determine the sand fractions and a densitometry technique based on Stokes law (Mériaux, 1953 and 1954) for the clay and silt fractions. The particle sizes of the Dunville, Elora and Cambridge samples were all measured using the hydrometer method (Bouyoucos, 1962). Liquid water content was measured using the drying and weighting technique for all soil samples (O'Kelly, 2004).

4 Results

4.1 Experimental results

Figures 5 to 8 show the complex permittivity of the four soil samples when undergoing consecutive freeze/thaw cycles. Of note, the freeze/thaw transitions were reproducible between cycles using both HP and OECP sensors. Hysteresis effects can be observed between the freezing and thawing cycles in Figs. 5 through 8. Although hysteresis should be expected because of the latent heat of fusion of water, this effect was amplified by the experimental setup and transition speed (Pardo Lara et al.; 2020). The HP measurements show very similar trends to the OECP measurements during freeze/thaw transitions, especially for the real permittivity. The fully frozen and thawed permittivity values are also similar between the OECP and HP measurements, with offsets depending on the soil type (Tables 2 and 3).

The OECP and HP permittivity measurements, compared in the scatterplots of Fig. 9, are similar for the real part (RMSE = 1.03) but show larger discrepancies for the imaginary part (RMSE = 1.82). The OECP measured imaginary part is, as expected, lower than that of the HP because at microwave frequencies the dielectric loss due to liquid water is more pronounced (Mätzler, 1987; Artemov and Volkov, 2014). It can

https://doi.org/10.5194/hess-2020-291
Preprint. Discussion started: 10 July 2020


Hydrology and Earth System Sciences
Discussions

also be observed that the freeze/thaw transition measurements are smoother with the HP than the OECP. This is partially due to the HP's larger probed volume. Since the instruments measure an average permittivity for the whole probed volume, a larger probed volume will record a smoother freeze/thaw transition because of the longer time required for the freezing/thawing fronts to penetrate the depth of volume probed.

4.2 Model Results

Soil parameters from Table 1 were used to drive the TD GRMDM and Zhang's model. Output from the models is shown in Figs. 5 to 9 and summarized in Tables 2 and 3. There are important discrepancies between the data and the models. The TD GRMDM does not simulate the freeze/thaw transition, resulting in a discontinuity in soil permittivity at the freezing point. Zhang's model estimates the ice fraction for a given sub-freezing temperature, displaying a smoother freeze/thaw transition. Even if amplified by the experimental setup, the hysteresis effect between the freezing and thawing cycles is not simulated by any model since they do not consider latent heat. The divergence between models and data is more prevalent for the imaginary part of the permittivity than for the real part. Zhang's model seems to systematically underestimate frozen soil permittivity, while the TD GRMDM fixed value approach is closer to the measured permittivity although it does not account, when the soil is frozen, for soil composition or ice content. Lastly, both models overestimated the soil permittivity of thawed samples with high water content according to the results of this study.

5 Discussion

The temperature dependence trend of permittivity during freeze/thaw transitions was similar across almost all OECP and HP measurements. The main difference between the permittivity measured at microwave and MHz frequencies appears to be an offset dependent on the soil type. Therefore, based on the offsets seen in Tables 2 and 3 and Fig. 9, a calibration equation between L-band and MHz permittivity can be obtained for a given soil. This would allow for the use of low-cost and widespread instrumentation in the MHz spectrum, such as the HP, to act as surrogate L-band soil permittivity measurements. This opens up the possibility of studies over large areas through already deployed networks. It should be remembered that MHz permittivity measurements have already been used to validate SMAP and SMOS algorithm's permittivity under the assumption that the MHz and L-band permittivity are equivalent (Roy et al., 2017a; Lemmetyinen et al., 2016). As our results showed, MHz and L-band soil permittivity trends are close to each other but not identical, therefore the previous assumption must be reconsidered because neglecting the frequency dependence of soil permittivity induces a bias in the results.

An important consideration in the use of devices for measuring the soil permittivity is the sample volume of the measurement. The HP and OECP instruments vary with respect to the soil volume probed. Ground-based and satellite-based L-band radiometric measurements are very sensitive to the freezing of the first centimetre of soil (Rowlandson et al., 2018; Roy et al., 2017a and 2017b; Williamson et al., 2018). Therefore, the

https://doi.org/10.5194/hess-2020-291
Preprint. Discussion started: 10 July 2020


Hydrology and Earth System Sciences
Discussions

shallower depth (~ 0.4–1 cm) and smaller volume (~4–10 cm^3) probed by the OECP makes it a more suitable instrument to study and understand the freeze/thaw signal observed from L-band radiometers.

The hysteresis effect observed in Figs. 5 to 8 was likely amplified by the experimental setup because of the fast temperature transition speed used. Nonetheless, the hysteresis effect is expected to occur because of the asymmetry between the freezing and thawing processes. The hysteresis is partially explained by the latent heat of fusion of water, that is to say that the soil does not start to freeze until the temperature is below freezing point and does not thaw until the temperature is over 0°C. Figure 10 demonstrates the hysteresis effect simulated by using a modified version of Zhang's model. The classic Zhang's model only takes into account ice fraction below 0°C. Zhang's model was modified to consider ice fraction above 0°C. This ice fraction was prescribed following an exponential function ($\frac{e^x}{e^x+1}$) around the freezing point. For a proper estimation of ice fraction in soil, the evolution of the soil and boundary conditions should be simulated using more complex models like CLASSIC (Melton at al., in review).

This hypothesis was tested on an OBS soil sample using a slower freeze/thaw transition rate. The hysteresis effect displayed in Fig. 11 is still noticeable (< 1°C offset from freezing point) but not as pronounced as in Figs. 5 to 8 (between 2°C and 3°C offset from freezing point). Since the soil permittivity has an important impact on brightness temperature as observed by satellite-based radiometers (Roy et al., 2017a and 2017b; Prince et al., 2019; Jonard et al., 2018), it is notable that this hysteresis effect around freezing point is not taken into account in current soil models used in microwave satellite retrieval algorithms. The omission of this effect may potentially have an impact on freeze/thaw detection products and their validation. It should be noted that this hysteresis effect is not always observed for *in situ* data due to the instrumental uncertainty not being precise enough to conclusively separate the hysteresis effect *in situ* (e.g. Pardo Lara et al., 2020). The effect might also be mitigated at the pixel scale of modern satellites because of spatial heterogeneity (Roy et al. 2017b).

Based on our simulations, ice fraction representation in Zhang's model results in a more physically appropriate representation of processes around the freezing point and results in smoother transitions. It should be noted that an ice fraction could be implemented in TD GRMDM as well. To reproduce the hysteresis effect at freeze/thaw transition, two approaches are possible. An empirical approach could be used by implementing a double threshold (variable for the freeze and the thaw cycle). This empirical approach would require determining the freezing/thawing temperature offset independently for each transition type which would depend on liquid water content, textural composition, solute concentration, and the pore pressure of the soil (Daanen et al., 2011). The alternative would be to couple dielectric models with soil physical models that integrate the time evolution of soil physical properties (e.g. CLASSIC model; Melton at al., in review). Soil physical models provide an estimate of the ice fraction through time, which is used by dielectric models

https://doi.org/10.5194/hess-2020-291
Preprint. Discussion started: 10 July 2020

to estimate soil permittivity. Such coupling should only impact the freeze/thaw transition where ice fraction is a relevant parameter.

6 Conclusions

The study shows that the open-ended coaxial probe (OECP) is a suitable device for measuring soil microwave permittivity in the same frequency range as the SMAP and SMOS satellites, as well as future L-band satellite missions. We also showed that lower frequency (MHz) soil permittivity probes can be used to estimate microwave permittivity given proper calibration relative to an L-band probe. This study also highlighted the need to improve dielectric soil models particularly during freeze/thaw transitions. We observed noticeable discrepancies between *in situ* data and model estimates, and no current model accounts for the hysteresis effect shown between freezing and thawing processes. Few studies have investigated this hysteresis effect, which could have a significant impact on freeze/thaw detection from satellites. Future work will look to improve soil thermal regime retrieval near the freezing point using permittivity measurements, which is impactful on the evaluation of the carbon budgets of northern regions.

7 Acknowledgments

This work was made possible thanks to the contributions of the Canadian Space Agency (CSA), Natural Sciences and Engineering Research Council of Canada (NSERC), Canada Foundation for Innovation (CFI). The experiments in Bordeaux were supported by the Samuel-De-Champlain France-Québec collaborative project (Fonds québécois de la recherche sur la nature et les technologies, FQRNT). We would also like to thank Bilal Filali, PhD, for his contribution to the design and manufacture of the probe, along with Simone Bircher, Arnaud Mialon, Yann Kerr and the entire CESBIO team in Toulouse for their contributions to probe testing and collaboration with Bordeaux laboratory. A special thanks to Jean-Pierre Wigneron from INRA for providing the codes to run the TD GRMDM model.

8 Competing interests

The authors declare that they have no conflict of interest.

9 Data availability

The research data can be accessed by direct request to the author.

https://doi.org/10.5194/hess-2020-291
Preprint. Discussion started: 10 July 2020

Hydrology and Earth System Sciences
Discussions

References

Artemov, V., and Volkov, A.: Water and Ice Dielectric Spectra Scaling at 0ºC, Ferroelectr., 466, 158–165, https://doi.org/10.1080/00150193.2014.895216, 2014.

Bircher, S., Anreasen, M., Vuollet, J., Vehviläinen, J., Raitiainen, K., Jonard, F., Weihermüller, L., Zakharova, E., Wigneron, J.-P., and Kerr, Y.: Soil moisture sensor calibration for organic soil surface layers, Geosci. Instrum. Methods Data Syst., 5, 109–125, https://doi.org/10.5194/gi-5-109-2016, 2016a.

Bircher, S., Demontoux, F., Razafindratsima, S., Bircher, S., Zakharova, E., Drusch, M., Wigneron, J.-P., and Kerr, Y.: L-Band Relative Permittivity of Organic Soil Surface Layers—A New Dataset of Resonant Cavity Measurements and Model Evaluation, Remote Sens., 8, 1024, https://doi.org/10.3390/rs8121024, 2016b.

Burns, T., Adams, J., and Berg, A.: Laboratory Calibration Procedures of the Hydra Probe Soil Moisture Sensor: Infiltration Wet-Up vs. Dry-Down, Vadose Zone J., 13(12), 1–10, https://doi.org/10.2136/vzj2014.07.0081, 2014.

Bouyoucos, G.: Hydrometer method improved for making particle size analysis of soils, Agron. J., 54(5), 464–465, https://doi.org/10.2134/agronj1962.00021962005400050028x, 1962.

Colliander, A., Jackson, T., Bindlish, R., Chan, S., Das, N., Kim, S., Cosh, M., Dunbar, R., Dang, L., Pashaian, L., Asanuma, J., Aida, K., Berg, A., Rowlandson, T., Bosch, D., Caldwell, T., Caylor, K., Goodrich, D., al Jassar, H., Lopez-Baeza, E., Martínez Fernández, J., González-Zamora, A., Livingston, S., McNairn, H., Pacheco, A., Moghaddam, M., Montzka, C., Notarnicola, C., Niedrist, G., Pellarin, T., Prueger, J., Pulliainen, J., Rautiainen, K., Ramos, J., Seyfried, M., Starks, P., Su, Z., Zeng, Y., van der Velde, R., Thibeault, M., Dorigo, W., Vreugdenhil, M., Walker, J. P., Wu, X., Monerris, A., O'Neill, P. E., Entekhabi, D., Njoku, E.G., and Yueha, S.: Validation of SMAP surface soil moisture products with core validation sites, Remote Sens. Environ., 191, 215-231, https://doi.org/10.1016/j.rse.2017.01.021, 2017.

Daanen, R., Misra, D., and Thompson, A.: Frozen Soil Hydrology. Encyclopedia of Snow, Ice and Glaciers, edited by: Singh, V., Singh, P., and Haritashya, U., Springer Netherlands, 306–11, 2011.

Demontoux, F., Razafindratsima, S., Bircher, S., Ruffié, G., Bonnaudin, F., Jonard, F., Wigneron, J.-P., Sbartaï, M., and Kerr, Y.: Efficiency of end effect probes for in-situ permittivity measurements in the 0.5–6 GHz frequency range and their application for organic soil horizons study, Sens. Actuators, A: Physical, 254, 78–88, https://doi.org/10.1016/j.sna.2016.12.005, 2017.

Demontoux, F., Tsague King, J., Bircher, S., Ruffie, G., Bonnaudin, F., Wigneron, J.-P., and Kerr, Y.: In-situ multi-frequency dielectric measurements to improve soil permittivity models for radiometric observations of soil in the high latitudes, Microrad 2020, Florence (Italy), Accepted.

Demontoux, F., Yaakoubi, G., Wigneron, G., Grzeskowiak, M., Sbartaï, M., Fadel, L., Ruffié, G., Bonnaudin, F., Oyhenart, L., Vignéras, V., Wigneron, J.-P., Villard, L., Le Toan, T., and Kerr, Y.: Antipodal Vivaldi antennas dedicated to in-situ broadband microwave permittivity measurements, 2019 European Microwave Conference in Central Europe (EuMCE), Prague (CzechRepublic), 62–65, https://prodinra.inra.fr/record/495910, 2019.

Derksen, C., Xu, X., Scott Dunbar, R., Colliander, A., Kim, Y., Kimball, J. S., Black, T. A., Euskirchen, E., Langlois, A., Loranty, M. M., Marsh, P., Rautiainen, K., Roy, A., Royer, A., and Stephens, J.: Retrieving landscape freeze/thaw state from Soil Moisture Active Passive (SMAP) radar and radiometer measurements, Remote Sens. Environ., 194, 48–62, http://dx.doi.org/10.1016/j.rse.2017.03.007, 2017.

https://doi.org/10.5194/hess-2020-291
Preprint. Discussion started: 10 July 2020

Dobson, M., Ulaby, F., Hallikainen, M., and El-Rayes, M.: Microwave dielectric behavior of wet soil - Part II: Dielectric mixing models, Geosci. Model Dev., GE-23, 35–46, https://doi.org/10.1109/TGRS.1985.289498, 1985.

Entekhabi, D., Njoku, E., O'Neill, P., Kellogg, K., Crow, W., Edelstein, W., Entin, J., Goodman, S., Jackson, T., Jackson, J., Kimball, J., Piepmeier, J., Koster, R., Martin, N., McDonald, K., Moghaddam, M., Moran, S., Reichle, R., Shi, J., Spencer, M., Thurman, S., Tsang, L., and Van Zyl, J.: The Soil Moisture Active Passive (SMAP) mission, Proc. of the IEEE, 98, 704–716, http://dx.doi.org/10.1109/JPROC.2010.2043918, 2010.

Fan, L., Wigneron, J.-P., Mialon, A., Rodriguez-Fernandez, N.J., Ai-Yaari, A., Kerr, Y., Brandt, M., and Ciais, P.: SMOS-IC Vegetation Optical Depth Index in Monitoring Aboveground Carbon Changes in the Tropical Continents During 2010–2016, IGARSS 2018 - 2018 IEEE International Geoscience and Remote Sensing Symposium, Valencia (Spain), 2825–2828, https://doi.org/10.1109/igarss.2018.8518750, 2018.

Filali, B., Boone, F., Rhazi, J.-E., Ballivy, G.: Design and calibration of a large open-ended coaxial probe for the measurement of the dielectric properties of concrete, IEEE Trans. Microwave Theory Tech., 56, 2322–2328, https://doi.org/10.1109/TMTT.2008.2003520, 2008.

Filali, B., Rhazi, J.-E., and Ballivy, G.: Measurement of the dielectric properties of concrete by a large coaxial probe with open end, Can. J. Phys., 84, 365–379, https://doi.org/10.1139/p06-056, 2006.

Gower S., Vogel, J., Norman, J., Kucharik, C., Steele, S., Stow, T.: Carbon distribution and aboveground net primary production in aspen, jack pine, and black spruce stands in Saskatchewan and Manitoba, Canada, J. Geophys. Res., 102(D24), 29029–29041, https://doi.org/10.1029/97JD02317, 1997.

HydraProbe Soil Sensor Manual, Revision VI, Stevens Water Monitoring Systems Inc., Portland, Oregon, United-States, 63 pp., 2018.

Jonard, F., Bircher, S., Demontoux, F., Weihermüller, L., Razafindratsima, S., Wigneron, J.-P., and Vereecken, H.: Passive L-Band Microwave Remote Sensing of Organic Soil Surface Layers: A Tower-Based Experiment, Remote Sens., 10(2), 304, https://doi.org/10.3390/rs10020304, 2018.

Kerr, Y., Waldteufel, P., Richaume, P., Wigneron, J., Ferrazzoli, P., Mahmoodi, A., Al Bitar, A., Cabot, F., Gruhier, C., Juglea, S., Leroux, D., Mialon, A., and Delwart, S.: The SMOS soil moisture retrieval algorithm, IEEE Trans. Geosci. Remote Sens., 50, 1384–1403, https://doi.org/10.1109/TGRS.2012.2184548, 2012.

Kerr, Y. H., Waldteufel, P., Wigneron, J. P., Delwart, S., Cabot, F. O., Boutin, J., Escorihuela, M. J., Font, J., Reul, N., Gruhier, C., and Juglea, S. E.: The SMOS mission: New tool for monitoring key elements of the global water cycle, IEEE Trans. Geosci. Remote Sens., 98, 666–687, https://doi.org/10.1109/JPROC.2010.2043032, 2010.

Kim, Y., Kimball, K., Zhang, K., and McDonald, K.: Satellite detection of increasing northern hemisphere non-frozen seasons from 1979 to 2008: implications for regional vegetation growth, Remote Sens. Environ., 121, 472-487, http://dx.doi.org/10.1016/j.rse.2012.02.014, 2012.

Klingshirn, C. F.: Semiconductor Optics – Graduate Texts in Physics (Chapter: Kramers–Kronig Relations), Springer, Berlin, Heidelberg, 849 pp., 2012.

Lemmetyinen, J., Schwank, M., Rautiainen, K., Kontu, A., Parkkinen, T., Mätzler, C., Wiesmann, A., Wegmüller, U., Derksen, C., Toose, P., Roy, A., and Pulliainen, J.: Snow density and ground permittivity retrieved from L-band radiometry: Application to experimental data, Remote Sens. Environ., 180, 377-391, https://doi.org/10.1016/j.rse.2016.02.002, 2016.

https://doi.org/10.5194/hess-2020-291
Preprint. Discussion started: 10 July 2020

Le Vine, D. M., Lagerloef, G. S., and Torrusio, S.: Aquarius and remote sensing of sea surface salinity from space, Proc. IEEE, 98, 688–703, https://doi.org/10.1109/JPROC.2010.2040550, 2010.

Mialon, A., Richaume, P., Leroux, D., Bircher, S., Bitar, A.A., Pellarin, T., Wigneron, J., and Kerr, Y.: Comparison of Dobson and Mironov Dielectric Models in the SMOS Soil Moisture Retrieval Algorithm, IEEE Trans. Geosci. Remote Sens., 53(6), 3084–3094, https://doi.org/10.1109/TGRS.2014.2368585, 2015.

Mätzler, C.: Applications of the interaction of microwaves with the natural snow cover, Remote Sens. Rev., 2, 259–387, https://doi.org/10.1080/02757258709532086, 1987.

Mavrovic, A., Madore, J.-B., Langlois, A., Royer, A., and Roy, A.: Snow liquid water content measurement using an open-ended coaxial probe (OECP), Cold Reg. Sci. Technol., 171, 102958, https://doi.org/10.1016/j.coldregions.2019.102958, 2020.

Mavrovic, A., Roy, A., Royer, A., Filali, B., Boone, F., Pappas, C., Sonnentag, O.: Dielectric characterization of vegetation at L band using an open-ended coaxial probe, Geosci. Instrum. Methods Data Syst., 7, 195–208, https://doi.org/10.5194/gi-7-195-2018, 2018.

Melton, J., Arora, V., Wisernig-Cojoc, E., Seiler, C., Fortier, M., Chan, E., and Teckentrup, L.: CLASSIC v1.0: the open-source community successor to the Canadian Land Surface Scheme (CLASS) and the Canadian Terrestrial Ecosystem Model (CTEM) – Part 1: Model framework and site-level performance, Geosci. Model Dev., https://doi.org/10.5194/gmd-2019-329, in review.

Mériaux, S.: Contribution à l'étude de l'analyse granulométrique, Thèses présentées à la faculté des sciences de l'université de Paris, Institut national de recherche agronomique, Paris (France), Série A, 590(614), 117 pp., 1953.

Mériaux, S.: Contribution à l'étude de l'analyse granulométrique, Ann. Agron., 5(I) 5–53 and 5(II) 149–205, 1954.

Mialon, A., Richaume, P., Leroux, D., Bircher, S., Bitar, A., Pellarin, T., Wigneron, J.-P., and Kerr, Y.: Comparison of Dobson and Mironov Dielectric Models in the SMOS Soil Moisture Retrieval Algorithm, IEEE Trans. Geosci. Remote Sens., 53(6), 3084–3094, https://doi.org/10.1109/TGRS.2014.2368585, 2015.

Mironov, V., De Roo, R., and Savin, I.: Temperature-Dependable Microwave Dielectric Model for an Arctic Soil, IEEE Trans. Geosci. Remote Sens., 48(6), 585–589, https://doi.org/10.1109/TGRS.2010.2040034, 2010.

Mironov, V., Kosolapova, L., and Fomin, S.: Physically and Mineralogically Based Spectroscopic Dielectric Model for Moist Soils, IEEE Trans. Geosci. Remote Sens., 47(7), 2059–2070, https://doi.org/10.1109/TGRS.2008.2011631, 2009.

Mironov, V., Kosolapova, L., Lukina, Y., Karavayskya, A., and Molostovb, I.: Temperature and texture-dependent dielectric model for frozen and thawed mineral soils at a frequency of 1.4 GHz, Remote Sens. Environ., 200, 240-249, https://doi.org/10.1016/j.rse.2017.08.007, 2017.

Mo, T., Choudhury, B., Schmugge, T., Wang, J., and Jackson, T.: A model for microwave emission from vegetation-covered fields, J. Geophys. Res., 87, 11229–11237, https://doi.org/10.1029/JC087iC13p11229, 1982.

Montpetit, B., Royer, A., Roy, A., and Langlois, A.: In-situ passive microwave emission model parameterization of sub-arctic frozen organic soils, Remote Sens. Environ., 205, 112-118, https://doi.org/10.1016/j.rse.2017.10.033, 2018.

Moradizadeh, M., and Saradjian, M.: The effect of roughness in simultaneously retrieval of land surface parameters. Phys. Chem. Earth, Parts A/B/C, 94, 127–135. https://doi.org/10.1016/j.pce.2016.03.006, 2016.

https://doi.org/10.5194/hess-2020-291
Preprint. Discussion started: 10 July 2020

O'Kelly, B.: Accurate Determination of Moisture Content of Organic Soils Using the Oven Drying Method, Drying Technol., 22(7), 1767–1776, http://dx.doi.org/10.1081/DRT-200025642, 2004.

Pavlov, N., and Baloshin, Y.: Electromagnetic properties of water on GHz frequencies for medicine tasks and metamaterial applications, J. Phys. Conf. Ser., 643, 012047, https://doi.org/10.1088/1742-6596/643/1/012047, 2015.

Pardo Lara, R., Berg, A., Warland, J., and Tetlock, E.: In Situ Estimates of Freezing/Melting Point Depression in Agricultural Soils Using Permittivity and Temperature Measurements, Water Resour. Res., 56(5), e2019WR026020, https://doi.org/10.1029/2019WR026020, 2020.

Prince, M., Roy, A., Royer, A., and Langlois, A.: Timing and spatial variability of fall soil freezing in boreal forest and its effect on SMAP L-band radiometer measurements, Remote Sens. Environ., 231, 111230, https://doi.org/10.1016/j.rse.2019.111230, 2019.

Rautiainen, K., Parkkinen, T., Lemmetyinen, J., Schwank, M., Wiesmann, A., Ikonen, J., Derksen, C., Davydov, S., Davydova, A., Boike, J., and Langer, M.: SMOS prototype algorithm for detecting autumn soil freezing, Remote Sens. Environ., 180, 346–360, https://doi.org/10.1016/j.rse.2016.01.012, 2016.

Rodríguez-Fernández, N. J., Mialon, A., Mermoz, S., Bouvet, A., Richaume, P., Al Bitar, A., Al-Yaari, A., Brandt, M., Kaminski, T., Le Toan, T., Kerr, Y. H., and Wigneron, J.-P.: An evaluation of SMOS L-band vegetation optical depth (L-VOD) data sets: high sensitivity of L-VOD to above-ground biomass in Africa, Biogeosciences, 15, 4627–4645, https://doi.org/10.5194/bg-15-4627-2018, 2018.

Rowlandson, T., Berg, A., Bullock, P., Ojo, E. R., McNairn, H., Wiseman, G., and Cosh, M.: Evaluation of several calibration procedures for a portable soil moisture sensor, J. Hydrol., 498, 335–344, https://doi.org/10.1016/j.jhydrol.2013.05.021, 2013.

Rowlandson, T., Berg, A., Roy, A., Kim, E., Pardo Lara, R., Powers, J., Lewis, K., Houser, P., McDonald, K., Toose, P., Wu, A., De Marco, E., Derksen, C., Entin, J., Colliander, A., Xu, X., and Mavrovic, A.: Capturing agricultural soil freeze/thaw state through remote sensing and ground observations: A soil freeze/thaw validation campaign, Remote Sens. Environ., 211, 59-70, https://doi.org/10.1016/j.rse.2018.04.003, 2018.

Roy, A., Royer, A., Derksen, C., Brucker, L., Langlois, A., Mialon, A., and Kerr, Y. H.: Evaluation of Spaceborne L-Band Radiometer Measurements for Terrestrial Freeze/Thaw Retrievals in Canada, IEEE J. Sel. Top. Appl. Earth Obs. Remote Sens., 8, 4442–4459, https://doi.org/10.1016/j.rse.2019.111542, 2015.

Roy, A., Toose, P., Williamson, M., Rowlandson, T., Derksen, C., Royer, A., Berg, A., Lemmetyinen, J., and Arnold, L.: Response of L-Band brightness temperatures to freeze/thaw and snow dynamics in a prairie environment from ground-based radiometer measurements, Remote Sens. Environ., 191, 67-80, https://doi.org/10.1016/j.rse.2017.01.017, 2017a.

Roy, A., Toose, P., Derksen, C., Rowlandson, T., Berg, A., Lemmetyinen, J., Royer, A., Tetlock, E., Helgason, W., and Sonnentag, O.: Spatial Variability of L-Band Brightness Temperature during Freeze/Thaw Events over a Prairie Environment, Remote Sens., 9, 894, https://doi.org/10.3390/rs9090894, 2017b

Roy, A., Leduc-Leballeur, M., Picard, G., Royer, A., Toose, P., Derksen, C., Lemmetyinen, J., Berg, A., Rowlandson, T., and Schwank, M.: Modelling the L-band snow-covered surface emission in a winter Canadian prairie environment, Remote Sens., 10, 1451, https://doi.org/10.3390/rs10091451, 2018.

Roy, A.R., Toose, P., Mavrovic, A., Pappas, C., Royer, A., Derksen, C., Berg, A., Rowlandson, T., El-Amine, M., Barr, A., Black, A., Langlois, A., and Sonnentag, O.: L-Band response to freeze/thaw in a

https://doi.org/10.5194/hess-2020-291
Preprint. Discussion started: 10 July 2020

boreal forest stand from ground- and tower-based radiometer observations, Remote Sens. Environ., 273, 111542, https://doi.org/10.1016/j.rse.2019.111542, 2020.

Seyfried, M., Grant, L., Du, E., and Humes, K.: Dielectric Loss and Calibration of the Hydra Probe Soil Water Sensor, Vadose Zone J., 4(4), 1070, https://doi.org/10.2136/vzj2004.0148, 2005.

Tetlock, E., Toth, B., Berg, A., Rowlandson, T., and Ambadan, J. T.: An 11-year (2007–2017) soil moisture and precipitation dataset from the Kenaston Network in the Brightwater Creek basin, Saskatchewan, Canada, Earth Syst. Sci. Data, 11(2), 787–796, https://doi.org/10.5194/essd-11-787-2019, 2019.

Wigneron, J.-P., Jackson, T. J., O'Neill, P., Lannoy, De, de Rosnay, P., Walker, J. P., Ferrazzoli, P., Mironov, V., Bircher, S., Grant, J. P., Kurum, M., Schwank, M., Munoz-Sabater, J., Das, N., Royer, A., Al-Yaari, A., Al Bitar, A., Fernandez-Moran, R., Lawrence, H., Mialon, A., Parrens, M., Richaume, P., Delwart, S., and Kerr, Y.: Modelling the passive microwave signature from land surfaces: a review of recent results and application to the L-band SMOS and SMAP soil moisture retrieval algorithms, Remote Sens. Environ., 192, 238–262, https://doi.org/10.1016/j.rse.2017.01.024, 2017.

Williamson, M., Rowlandson, T., Berg, A., Roy, A., Toose, P., Derksen, C., Arnold, L., and Tetlock, E.: L-band radiometry freeze/ thaw validation using air temperature and ground measurements. Remote Sens., 9(4), 403–410, https://doi.org/10.1080/2150704X.2017.1422872, 2018.

Zhang, L., Shi, J., Zhang, Z., and Zhao, K.: The estimation of dielectric constant of frozen soil-water mixture at microwave bands. IGARSS 2003. 2003 IEEE International Geoscience and Remote Sensing Symposium. Proceedings (IEEE Cat. No.03CH37477), Toulouse (France), 4, 2903–2905, https://doi.org/10.1109/IGARSS.2003.1294626, 2003.

Zhang, L., Zhao, T., Jiang, L., and Zhao, S.: Estimate of phase transition water content in freeze–thaw process using microwave radiometer, IEEE Trans. Geosci. Remote Sens., 48(12), 4248–4255, https://doi.org/10.1109/TGRS.2010.2051158, 2010.

https://doi.org/10.5194/hess-2020-291
Preprint. Discussion started: 10 July 2020

Hydrology and Earth System Sciences
Discussions
Open Access
EGU

625 **Figures**

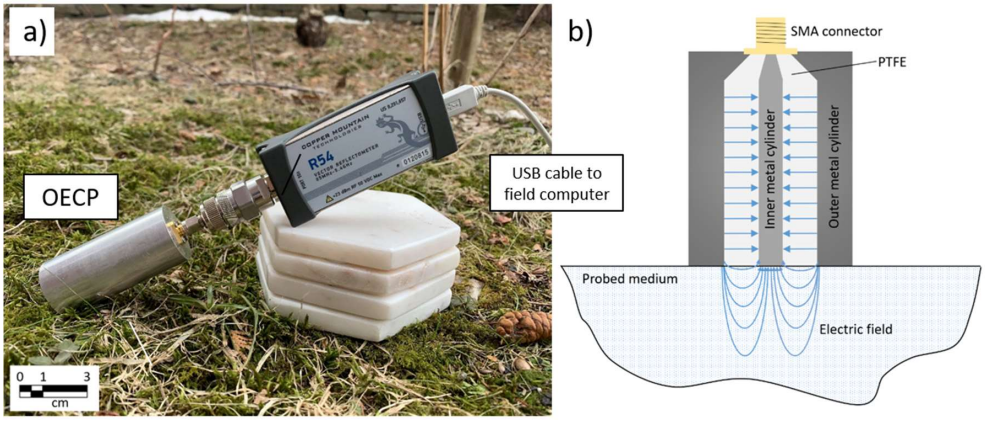

Figure 1: (a) OECP for permittivity measurement. The control program provided by the Planar R54 reflectometer manufacturer is operated with a field computer. The probe is connected to the Planar R54 reflectometer using a SMA/N cable or adaptor. (b) Diagram of the electrical field produced by the OECP.

630

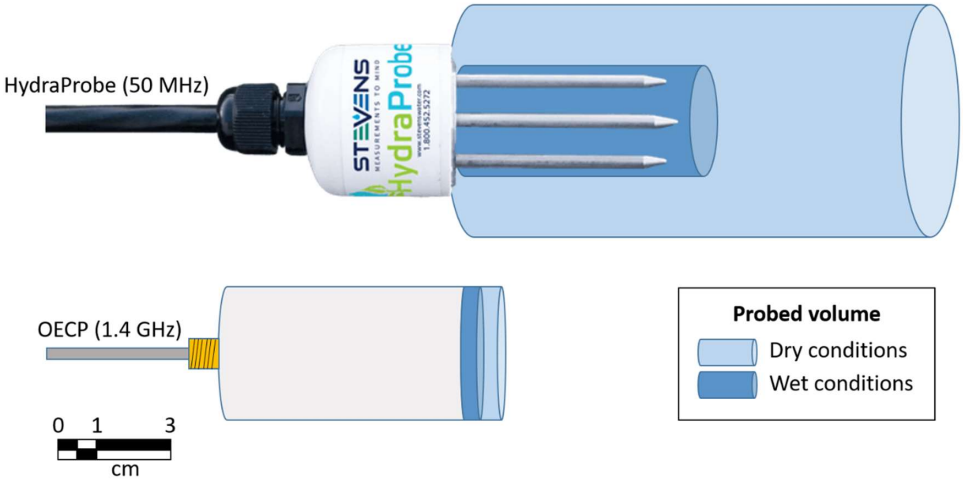

635 **Figure 2: Approximate probed volume (blue) of the HydraProbe (top) and OECP (bottom) for relatively dry and wet soil conditions. The probed volume is also influenced by soil type.**

https://doi.org/10.5194/hess-2020-291
Preprint. Discussion started: 10 July 2020

Hydrology and Earth System Sciences
Discussions
Open Access
EGU

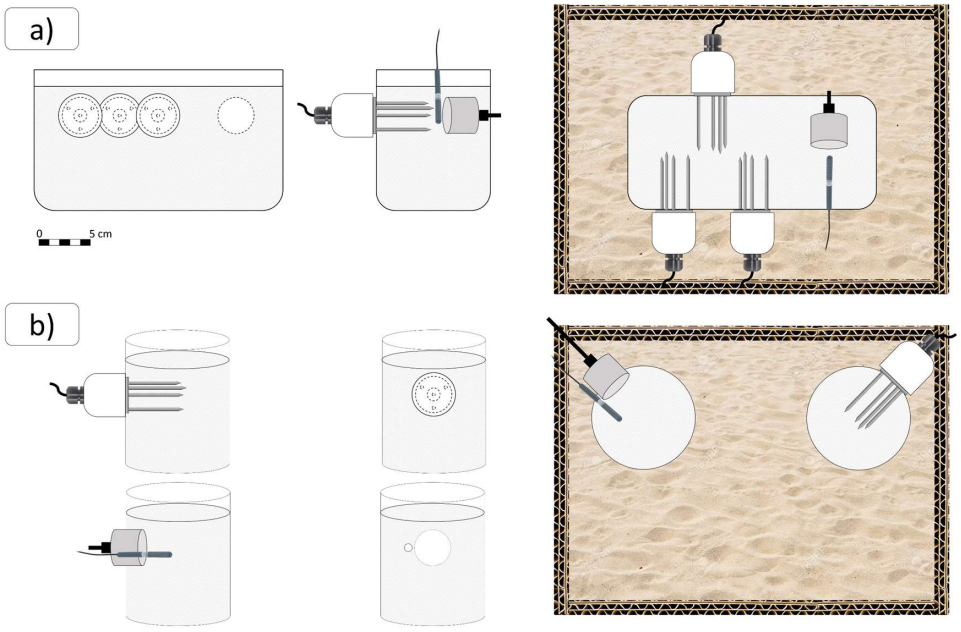

Figure 3: Top view of the cold chamber experimental setup at Guelph University (Ontario, Canada) for fast transition experiment. Setup for (a) the OBS sample, 11x24x12cm for a volume of $3.2x10^3$ cm^3 and (b) the Ontario samples, height of 12 cm and diameter of 10 cm for a volume of $9.4x10^2$ cm^3.

640

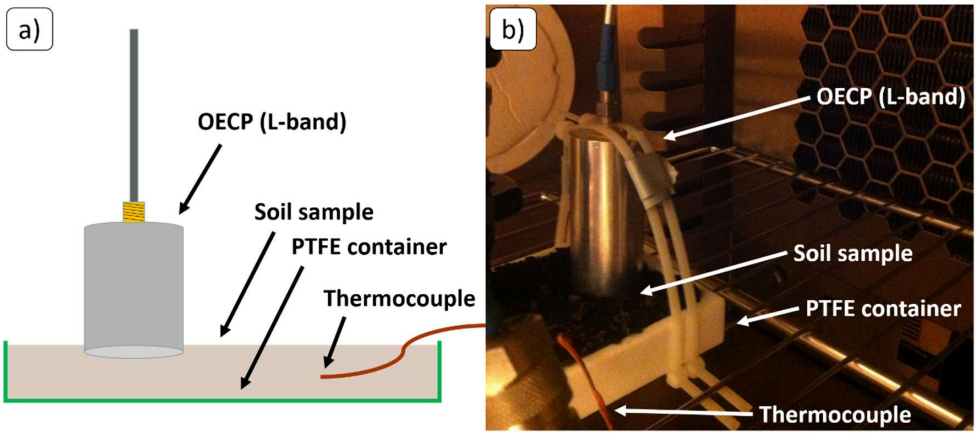

Figure 4: (a) Side view and (b) photo of the cold chamber experimental setup at the Laboratoire de l'Intégration du Matériau au Système (Bordeaux, France) for the slow freeze/thaw transition.

645

https://doi.org/10.5194/hess-2020-291
Preprint. Discussion started: 10 July 2020

Hydrology and Earth System Sciences
Discussions
Open Access
EGU

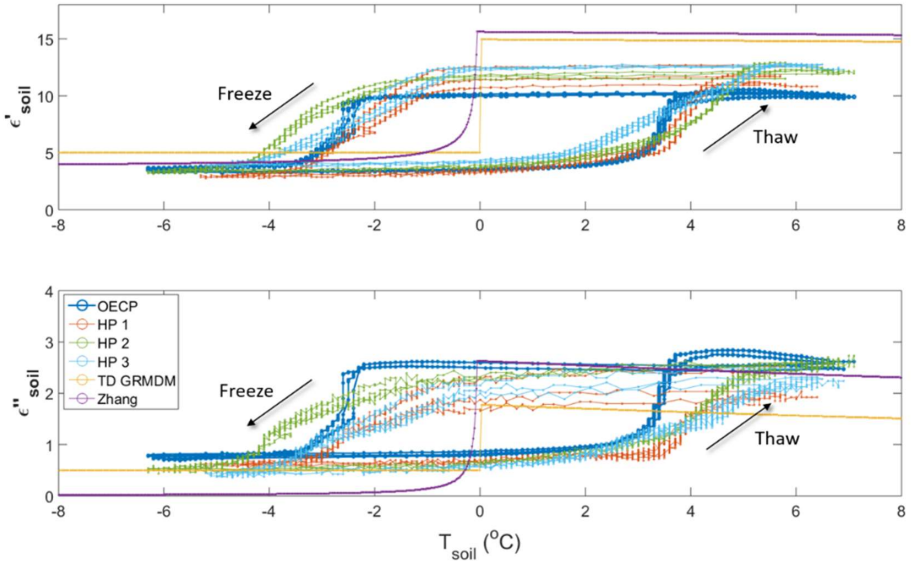

Figure 5: Real (ε') and imaginary (ε'') permittivity of an organic soil sample from the Old Black Spruce site (see Table 1) during freeze/thaw cycles in a cold chamber environment. The OECP and HP instruments monitored soil permittivity, where TD GRMDM and Zhang are model results. The hysteresis effect displayed here is amplified by the experimental setup (discussed in the text).

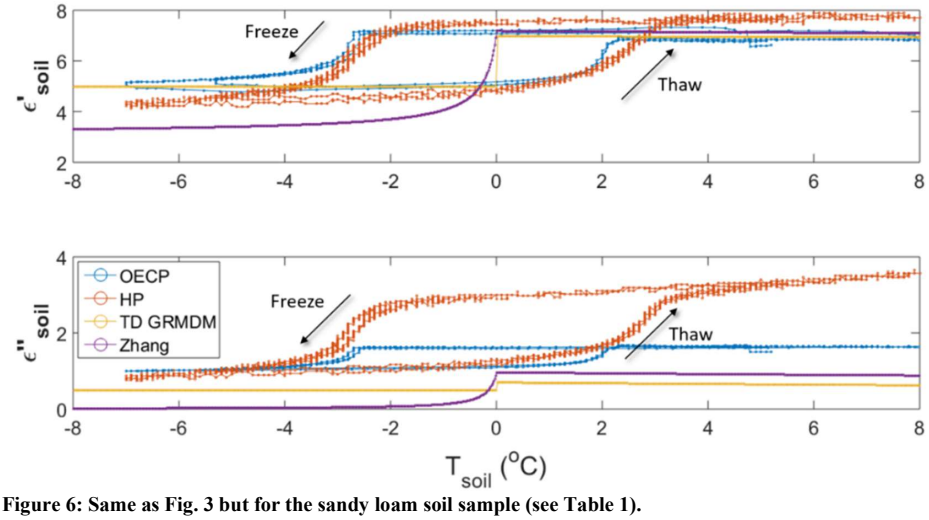

Figure 6: Same as Fig. 3 but for the sandy loam soil sample (see Table 1).

https://doi.org/10.5194/hess-2020-291
Preprint. Discussion started: 10 July 2020

Hydrology and Earth System Sciences
Discussions
Open Access
EGU

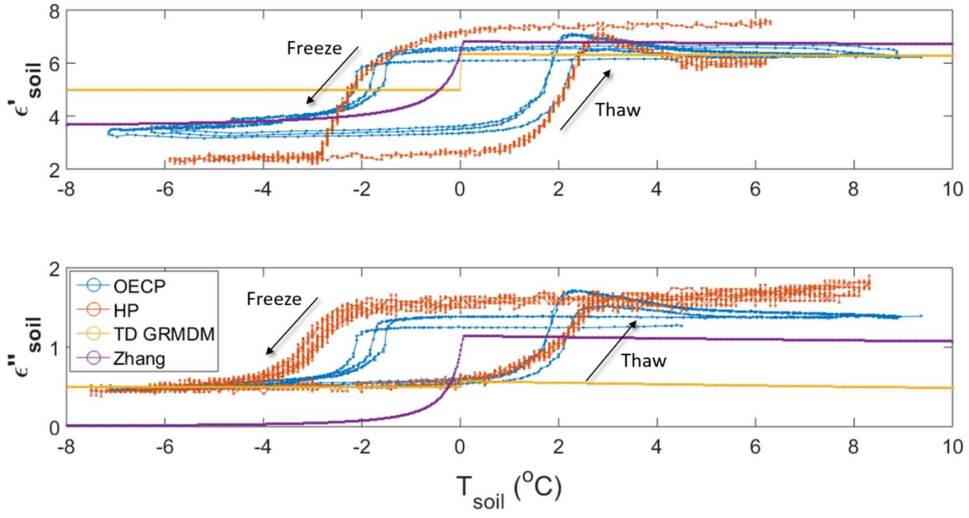

Figure 7: Same as Fig. 3 but for the loamy sand soil sample (see Table 1).

655

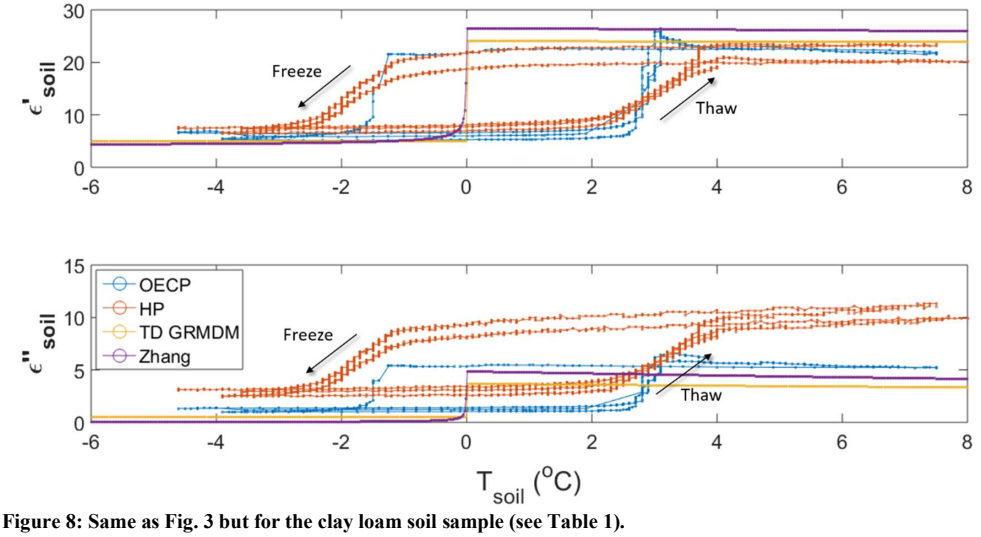

Figure 8: Same as Fig. 3 but for the clay loam soil sample (see Table 1).

https://doi.org/10.5194/hess-2020-291
Preprint. Discussion started: 10 July 2020

Hydrology and Earth System Sciences
Discussions

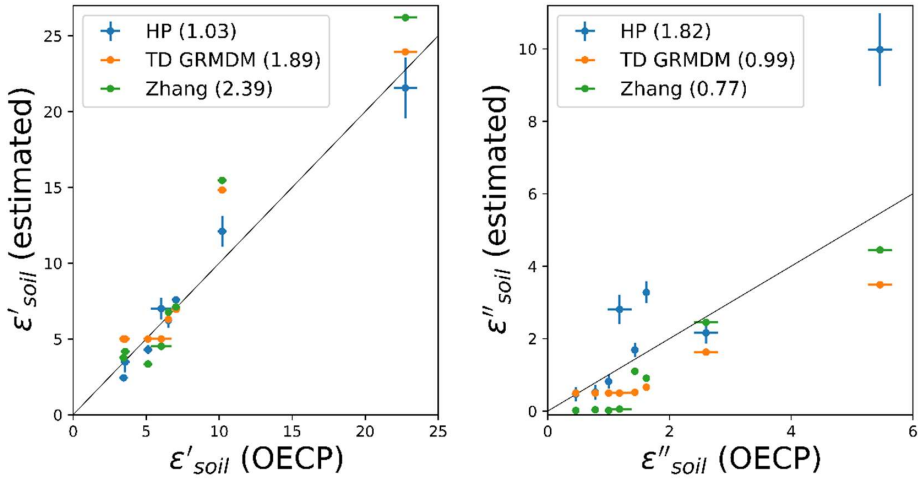

Figure 9: OECP real (ε') and imaginary (ε'') permittivity compared to HP (instrument), TD GRMDM (model) and Zhang (model) with the OECP as the reference. The black line is the 1:1 reference ratio and the root-mean square error is given in parentheses (RMSE).

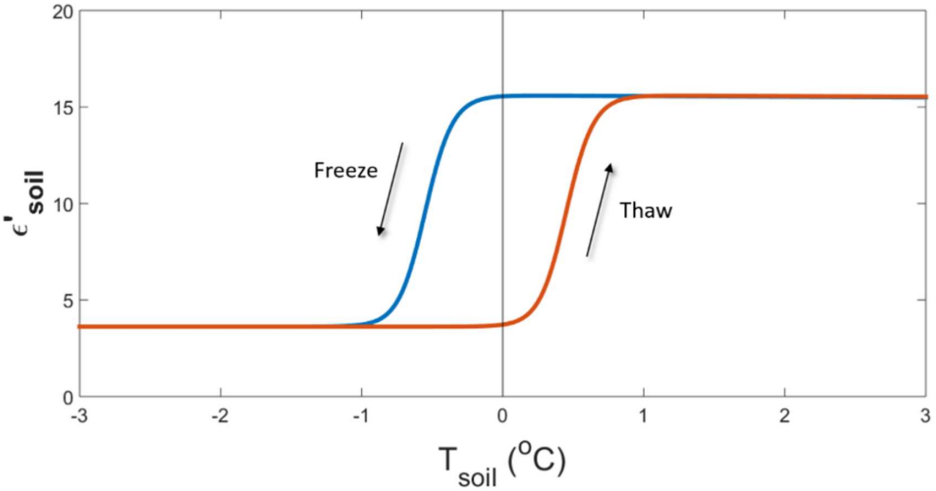

Figure 10: Expected hysteresis effect between freeze and thaw cycles. This theoretical curve was produced using an adapted version of Zhang's model and the soil composition of the OBS sample.

https://doi.org/10.5194/hess-2020-291
Preprint. Discussion started: 10 July 2020

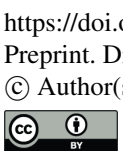

Hydrology and Earth System Sciences
Discussions
Open Access
EGU

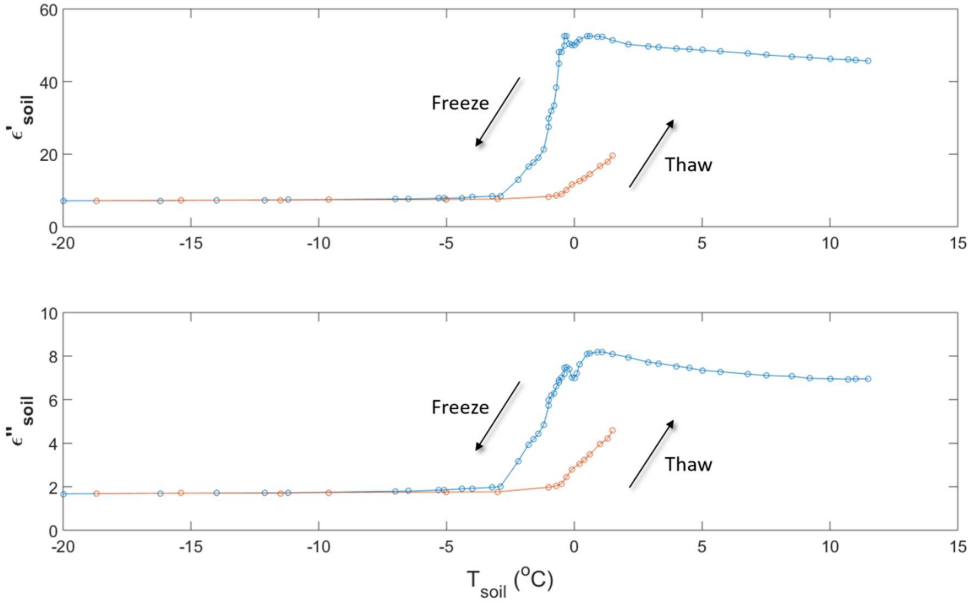

Figure 11: (a) Real (ε') and imaginary (ε'') permittivity of an organic soil sample from the Old Black Spruce site (collected May 3rd, 2017) during a slow freeze/thaw cycle in a cold chamber environment. (b) The OECP placed on top of an OBS soil sample to monitor soil permittivity in the Laboratoire de l'Intégration du Matériau au Système (Bordeaux, France).

https://doi.org/10.5194/hess-2020-291
Preprint. Discussion started: 10 July 2020

Hydrology and Earth System Sciences
Discussions
Open Access
EGU

Tables

Table 1: Soil composition and physical properties. The Old Black Spruce site is located in the boreal forest in Saskatchewan, Canada, and the three other sites are located in agricultural fields in southern Ontario, Canada. θ_V and θ_G stands for volumetric and gravimetric liquid water content, respectively. ρ_d stands for dry bulk density.

			Gravimetric composition				Physical properties		
Soil type	Site	Lattitude/ Longitude	Organic	Clay	Sand	Silt	θ_V	θ_G	ρ_d
			%	%	%	%	m^3/m^3	kg/kg	kg/m^3
Organic	Old Black Spruce	53°59′ N 105°07′ W	59	2.36	29.85	8.79	0.30	0.83	356.2
Sandy Loam	Elora	43°39′ N 80°25′ W	N/A	10	54	36	0.115	0.079	1450
Loamy Sand	Cambridge	46°26′ N 80°20′ W	N/A	2.5	78.4	19.1	0.068	0.038	1780
Clay Loam	Dunville	42°52′ N 79°44′ W	N/A	28	33	39	0.42	0.30	1400

Table 2: Modelled and measured complex permittivity of thawed soils. The permittivity in the 5°C to 6°C temperature range (stable plateau) is averaged over the multiple freeze/thaw cycles depicted in Figs. 5 through 8. Uncertainties (in parentheses) are based on instrument precision and measurement variability.

Soil type	$\varepsilon'_{thawed\ soil}$				$\varepsilon''_{thawed\ soil}$			
	OECP	HP	TD GRMDM	Zhang	OECP	HP	TD GRMDM	Zhang
Organic	10.2 (±0.3)	12.1 (±1.0)	14.83	15.46	2.6 (±0.2)	2.2 (±0.3)	1.63	2.45
Sandy Loam	7.0 (±0.3)	7.6 (±0.2)	6.95	7.12	1.62 (±0.04)	3.3 (±0.3)	0.66	0.91
Loamy Sand	6.5 (±0.2)	6.2 (±0.5)	6.30	6.77	1.43 (±0.05)	1.7 (±0.2)	0.52	1.10
Clay Loam	22.8 (±0.8)	21.7 (±2.0)	23.94	26.20	5.7 (±0.2)	10.0 (±1.0)	3.49	4.45

Table 3: Same as Table 2 but for frozen conditions (-5° to -6°C).

Soil type	$\varepsilon'_{frozen\ soil}$				$\varepsilon''_{frozen\ soil}$			
	OECP	HP	TD GRMDM	Zhang	OECP	HP	TD GRMDM	Zhang
Organic	3.6 (±0.3)	3.5 (±0.7)	5	4.17	0.78 (±0.04)	0.5 (±0.2)	0.5	0.039
Sandy Loam	5.1 (±0.3)	4.3 (±0.3)	5	3.35	1.00 (±0.04)	0.8 (±0.2)	0.5	0.020
Loamy Sand	3.5 (±0.3)	2.4 (±0.2)	5	3.76	0.46 (±0.04)	0.47 (±0.2)	0.5	0.017
Clay Loam	6.0 (±0.7)	7.0 (±0.7)	5	4.51	1.2 (±0.2)	2.8 (±0.4)	0.5	0.055